Experimental data imaging for the airborne bistatic SAR

XU Sanyuan, WANG Jianguo

School of Electronic Engineering, *University of Electronic Science and Technology of China*, *Sichuan Chengdu* 610054, *China*

Abstract: The signal processing in the bistatic SAR case is more complex than the monostatic synthetic aperture radar (SAR) case due to issues such as the range history of the target echo signal, time synchronization error, time-varying Doppler rate because of squint, etc. In this paper, a monostatic equivalent geometry model of bistatic SAR is established; the mechanism of the System time synchronization error is analyzed; a time synchronization error correction method based on direct-path signal is presented; a modified time-varying step transform algorithm is used for bistatic SAR. Theoretical analysis and experimental data processing confirmed the effectiveness of the algorithm.

Key words: bistatic, synthetic aperture radar, time synchronization, imaging algorithm

CLC number: TP958 **Document code:** A

Citation format: Xu S Y, Wang J G. 2010. Experimental data imaging for the airborne bistatic SAR. *Journal of Remote Sensing*. **14**(2): 262—271

1 INTRODUCTION

Bistatic synthetic aperture radar (BiSAR) is a radar system which mounts transmitter and receiver on different platforms. Because of this separation, BiSAR has several operational advantages such as more flexibility, safety and plenty of information in space domain, time domain and doppler domain, which make BiSAR more widely used than monostatic SAR. However, the complexity of BiSAR in structure leads to more difficulty in imaging processing. In recent years, BiSAR has become a research hotspot (Zhang & Yang, 2008; Zhu *et al*., 2007; Zhou & Pi , 2008).

In BiSAR system, transmitter and receiver are separated on different platforms, which respectively have independent frequency sources, so there are space radiation synchronization, time synchronization, phase synchronization and other issues. Krieger and Younis (2006) has investigated the impact of the uncompensated phase noise which may cause a time variant shift, spurious sidelobes and a deterioration of the impulse response, as well as a low-frequency phase modulation of the focused SAR signal. Therefore, phase mismatch should be ensured in the permissible scope.

The pulse repetition cycle of the transmitted signal could not equal the cycle of the reception window of the receiver, which maybe results in the problem of time synchronization. Due to the time synchronization error, the location of the echo data in data array does not reflect the radar, target distance changes. Johnsen(2002)and Weiβ(2004) presented a program which used GPS or two-way satellite time transfer to resolve the problem. Guo and Chen (2002) have developed a novel method of time synchronization for bistatic radar system via satellite TV field sync signal. In Germany, FGAN-FHR carried out a joint spaceborne and airborne SAR technology which involves inertial navigation system (INS), DGPS and TIRA for space radiation synchronization and time synchronization, direct-path signal for Trigger synchronization (Espeter *et al*., 2007). These methods all concentrated on how to obtain time synchronization while SAR is radiating. Actually, we can also correct time synchronization error to obtain SAR image during processing SAR data.

There are two different BiSAR patterns in working, which are time-varying pattern and time-invariant pattern respectively. Considering the requirement of imaging and the complexity of computation, it is clear that different patterns require different imaging algorithms. Back-projection (BP) algorithm can be considered as a simplified two-dimensional matched filtering algorithm which has a good robust and flexibility (Ding & Munson, 2002); polar formatting algorithm (PFA) also has good flexibility but with a smaller imaging scene (Rigling & Moses, 2004); non-linear chirp scaling (NLCS) has been developed in a variety of imaging models (Chen *et al*. 2008). Seismic wave equation was used to transform bistatic SAR echo data into equivalent monostatic SAR echo data (D'Aria *et al*. 2004), but the algorithm is only suited for the geometric model of Along Track (transceiver platforms fly along the same track, in the same direction with the same speed). He *et al*. (2005) proposed a wave-number domain BiSAR imaging algorithm. However, with increase in squint angle, the range-walk has a sharp increase. After range-walk removal, the data array

Received: 2009-02-05; **Accepted**: 2009-05-04

Foundation: National Natural Science Foundation (No.60772144).

First author biography: XU Sanyuan(1969—), male, lecturer, received the B.Sc. degree in Radio Communication Engineering from the Air Force Engineering University in 1993. He is pursuing the Ph.D. degree in University of Electronic Science and Technology of China. His current research interests are in SAR system and signal processing. He has published five papers. E-mail: xsy820@sohu.com

has a large number of zero, so wave number domain algorithm therefore can not deal with data of high squint BiSAR.

2 BISAR ECHO MODEL

2.1 Range history equivalent model transform

As shown in Fig.1 (a), the geometry of a constant, parallel flight BiSAR model is presented. There are two platforms which are S_T for transmitting and S_R for receiving respectively. The platforms move at the same constant velocity v_B; the height is h_T for transmitter, h_R for receiver. Assume that at azimuthal time zero the slant range from the center of scene to transmitter is R_T, the slant range from the center of scene to receiver is R_R. The spatial squint angle is θ_T, θ_R, defined as the complementary angle between radar line of sight and the direction of flight. The BiSAR instant range at time t is defined as

$$R_B(t)=\sqrt{v_B^2t^2+R_T^2-2v_BtR_T\cos(\pi/2-\theta_T)}+\sqrt{v_B^2t^2+R_R^2-2v_BtR_R\cos(\pi/2-\theta_R)} \tag{1}$$

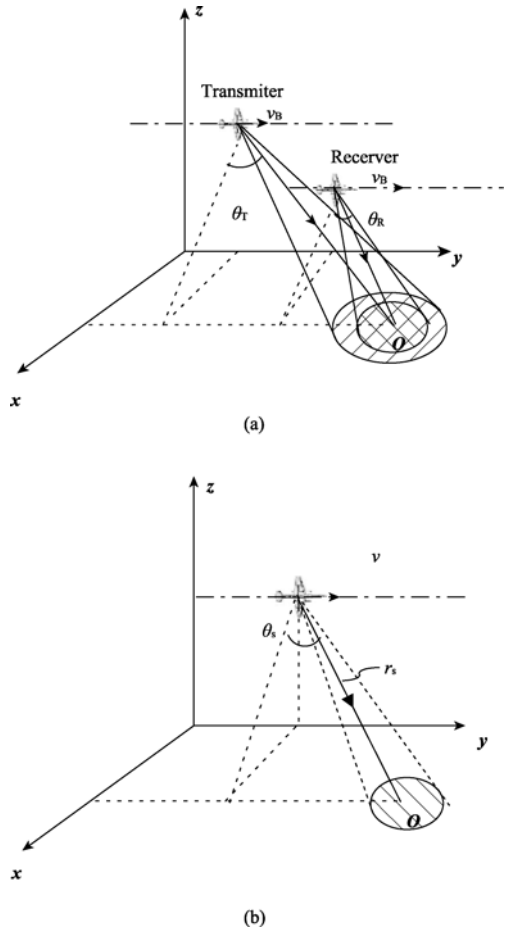

Fig. 1 (a) Bistatic SAR geometry model; (b) Bistatic SAR equivalent model

Eq. (1) can be expanded into its Taylor series as

$$R_B(t)=(R_T+R_R)-(\sin\theta_T+\sin\theta_R)v_Bt+\frac{1}{2}\left(\frac{\cos^2\theta_T}{R_T}+\frac{\cos^2\theta_R}{R_R}\right)v_B^2t^2+\frac{1}{2}\left(\frac{\cos^2\theta_T\sin\theta_T}{R_T^2}+\frac{\cos^2\theta_R\sin\theta_R}{R_R^2}\right)v_B^3t^3 \tag{2}$$

The time-invariant pattern BiSAR can be equivalent to a monostatic SAR illustrated as Fig. 1(b). The equivalent instant range of SAR to a target at O is

$$R(t)=\sqrt{v^2t^2+r_s^2-2vtr_s\cos(\pi/2-\theta_s)}\approx r_s-vt\sin\theta_s+\frac{1}{2r_s}v^2t^2\cos^2\theta_s+\frac{1}{2r_s^2}v^3t^3\cos^2\theta_s\sin\theta_s \tag{3}$$

where

$$\begin{cases}r_s=(R_T+R_R)/2\\ v=\dfrac{v_B}{2}\sqrt{2+2\sin\theta_T\sin\theta_R+\dfrac{R_R}{R_T}\cos^2\theta_T+\dfrac{R_T}{R_R}\cos^2\theta_R}\\ \theta_s=\sin^{-1}\left(\dfrac{v_B\sin\theta_R+v_B\sin\theta_T}{2v}\right)\end{cases} \tag{4}$$

2.2 Analysis of Echo Signal

Assume the transmitting signal is

$$s(t,\tau)=\sum_{n=0}^{N}\mathrm{rect}\left(\frac{t-nT_s}{T}\right)\exp(\mathrm{j}2\pi(f_0\tau+K\tau^2/2)) \tag{5}$$

where, t denotes azimuthal time, 'slow time'. τ denotes time in pulse, 'fast time'. T denotes the pulse duration, T_s denotes the pulse repetition interval (PRI) of transmitting, f_0 denotes carrier frequency and K denotes the LFM rate. The instant equivalent range from SAR to point target is $R(t)$, ξ=2$R(t)$/C, C denotes light velocity. Assume A denotes the amplitude accounting for propagation attenuation. The reflected signal will be

$$s(t,\tau-\xi)=\sum_{n=0}^{N}\mathrm{A}\ \mathrm{rect}\left(\frac{t-nT_s-\xi}{T}\right)\times\exp(\mathrm{j}2\pi(f_0(\tau-\xi)+K(\tau-\xi)^2/2)) \tag{6}$$

If there are M targets, by superposition, the return signal from scatters is given by

$$s_0(t,\tau)=\sum_{n=0}^{N}\sum_{m}^{M}A_m\mathrm{rect}\left(\frac{t-nT_s-\xi_m}{T}\right)\times\exp(\mathrm{j}2\pi(f_0(\tau-\xi_m)+K(\tau-\xi_m)^2/2)) \tag{7}$$

Due to the window of receiver sampling, the return signal will be

$$s_0(t,\tau)=\sum_{n=0}^{N}\mathrm{rect}\left(\frac{t-nT_r+\sigma}{T_w}\right)\times\sum_{\mathrm{m}}^{\mathrm{M}}A_m\mathrm{rect}\left(\frac{t-nT_s-\xi_m}{T}\right)\times\exp(\mathrm{j}2\pi(f_0(\tau-\xi_m)+K(\tau-\xi_m)^2/2)) \tag{8}$$

where, T_r denotes the repetition interval of window of sampling,

T_w denotes the duration of window, and σ denotes a constant reference time delay. For monostatic SAR, T_r=T_s; but for bistatic SAR, perhaps T_r≠T_s. While T_r≠T_s, $n(T_r-T_s)$ denotes the time synchronization error. After the range-compression is performed, for the m^{th} point target' peak response in data array occurs at

$$p_m(n)=\frac{T_w}{2}+n(T_r-T_s)-\sigma-\xi_m \tag{9}$$

Suppose the range between transmitter and receiver in BiSAR is ςC, and is the function of t. Then the signal via direct-path between transmitter and receiver will be

$$s_{rt}(t,\tau)=\sum_{n=0}^{N}\mathrm{rect}\left(\frac{t-nT_r+\sigma}{T_w}\right)\mathrm{A}\ \mathrm{rect}\left(\frac{t-nT_s-\varsigma}{T}\right)\times \exp(\mathrm{j}2\pi(f_0(\tau-\varsigma)+K(\tau-\varsigma)^2/2)) \tag{10}$$

Through the same processing, it can be seen that peak response in data array occurs at

$$p_{rt}(n)=\frac{T_w}{2}+n(T_r-T_s)-\sigma-\varsigma \tag{11}$$

Eq.(11) represents that the location of direct-path signal peak response in matrix depends upon ς and $n(T_r-T_s)$.

3 TIME SYNCHRONIZATION ERROR CORRECTION

Because the amplitude of direct path signal is stronger than that of target signal and hardly influenced by other targets echo, it is convenience to shift in range and track azimuthal phase. An approach of time synchronization error correction by using direct-path signal is presented. The first align data array: Align data array in order to direct-path signal peak response locate in a straight line, and other data shift in the same way in data array. Thus the location of direct-path signal peak response in matrix is

$$\begin{aligned}p_{rt}^{'}(n)&=\left\{\frac{T_w}{2}+n(T_r-T_s)-\sigma-\varsigma\right\}-\left\{n(T_r-T_s)-\varsigma\right\}\\&=\frac{T_w}{2}-\sigma\end{aligned} \tag{12}$$

For other target, the location of signal peak response in matrix will occur at

$$\begin{aligned}p_m^{'}(n)&=\left\{\frac{T_w}{2}+n(T_r-T_s)-\sigma-\xi_m\right\}-\left\{n(T_r-T_s)-\varsigma\right\}\\&=\left\{\frac{T_w}{2}-\sigma-\xi_m\right\}+\varsigma\end{aligned} \tag{13}$$

Pick up the azimuthal phase of the direct-path signal, so that we can obtain the relative range between transmitter and receiver. The azimuthal phase of the direct-path signal is phase = $-2\pi f_0\varsigma$, then we calculate ς = –phase/$2\pi f_0$.

The second align data array: Align data array again, and let data array shift according to ς. Then the location of direct-path signal peak response in array is

$$p_{rt}^{''}(n)=\frac{T_w}{2}-\sigma-\varsigma \tag{14}$$

For other targets, the location of signal peak response in array will occur at

$$p_m^{''}(n)=\frac{T_w}{2}-\sigma-\xi_m \tag{15}$$

Thus, the processed data array will be decided by the range from transmitter to target and back to the receiver only, and the impact of time synchronization error could be eliminated.

The flow chart is as shown in Fig.2.

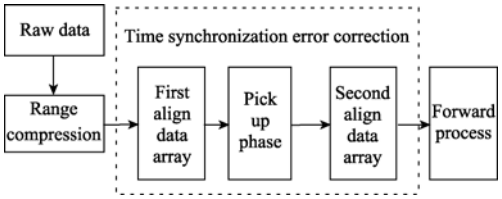

Fig. 2 Flow chart of time synchronization error correction

4 BISAR TIME-VARYING STEP-TRANSFORM ALGORITHM

In squint model, compared to the depth of focus, the range-cell migration is much larger, which means that we can not use a constant chirp rate to deramp all the subapertures in a range cell. Therefore, only time-varying sub-aperture imaging technique can adapt to large squint SAR imaging having large range walk (Sun *et al.*, 1999). After the completion of range compression, range-walk removal is needed in data array. Then we may think that the data of one target is lying in the same range cell. The first step of the procedure of focusing azimuthal data is linear phase compensation. The received data is divided into many subapertures and we have different deramping rates for different subapertures. That means reference functions are time-varying. Then Fourier transform of the deramped data within each subaperture results in the coarse resolution. After first FFT, selecting all the data belonging to one target from different subapertures and range cells, the phase compensation of these data is performed. The full-resolution image of the target can be obtained by making a fine-resolution FFT. In order to avoid frequency leak, subaperture is overlapping, therefore, output signal of fine-resolution FFT should be selected. Flow chart of the algorithm is shown in Fig.3.

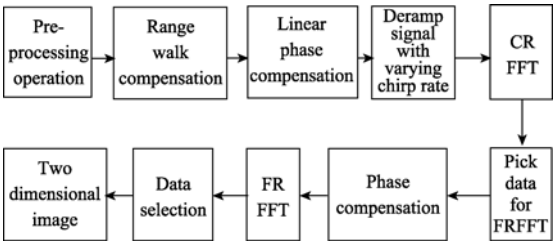

Fig. 3 Time-varying step-transform algorithm

5 BISAR EXPERIMENTAL DATA PROCESSING

Fig.4 is the image of part of BiSAR range compressed data without time synchronization error correction. Fig.5 is the relative range by computing the phase of signal of direct-path between transmitter and receiver, which is the mirror of instant distance of transceiver platforms. Fig.6 is the image of part of BiSAR range compressed data after time synchronization error correction. After time synchronization error correction shown in Fig.3, processing using time-varying step-transform algorithm, the final grayscale image is obtained shown in Fig.7.

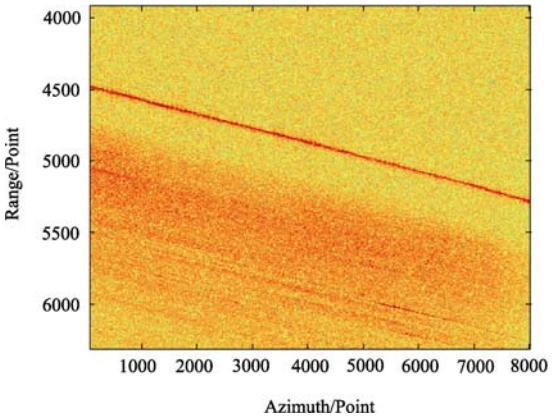

Fig. 4 BiSAR data before correction

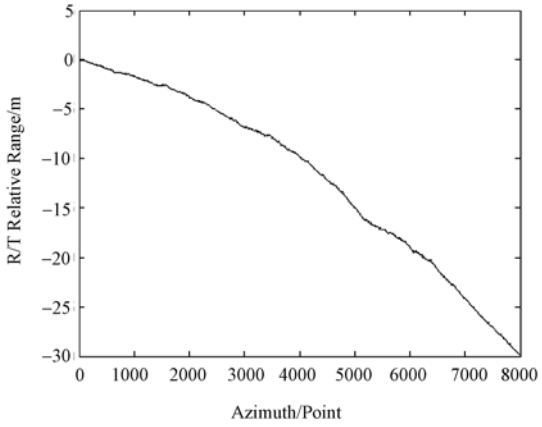

Fig. 5 Relative range between transmitter and receiver

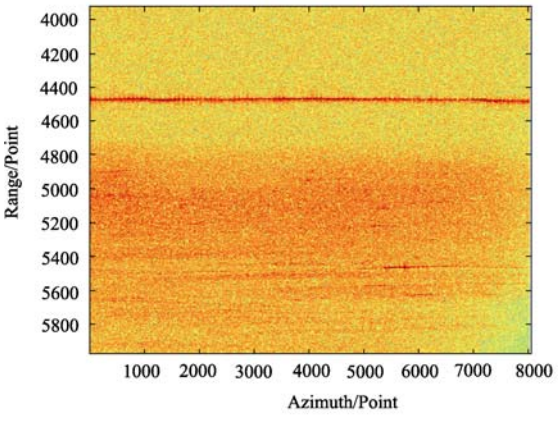

Fig. 6 BiSAR data after correction

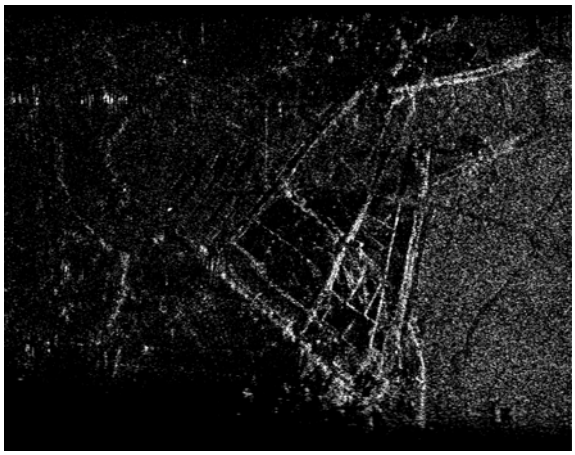

Fig. 7 BiSAR image

As can be seen from Fig.4, due to the existence of time synchronization error, the arrangement of echo data could not reflect the change in slant range. The stronger curve in figure is the image of direct-path signal after range compression. The range migration is nearly up to 850 range cells. But in Fig.5, the relative distance between two platforms has a change about 30 m, nearly 20 range cells during observation process. So the relative motion between platforms must not be ignored, and we could not align the direct-path signal data in a straight line simply and should separate the impact due to time synchronization error or due to the movement between two platforms. Furthermore, in Fig.7 we can see information has lost for time synchronization error.

In addition, because the algorithm has used the phase of direct-path signal to obtain the relative distance between the two platforms, there may be problem when the platforms is too drastic fluctuation, such as the aircraft turning, which could result Doppler frequency over PRF. Thus the phase can not reflect the change of the relative distance. The algorithm will fail. But in the meantime, reconnaissance imaging is usually not suitable.

6 CONCLUSION

In BiSAR, the slant range history of the echo signal is different from monostatic SAR, so the imaging algorithm of conventional SAR can not be directly used in BiSAR. This paper put forwards an equivalent model for BiSAR, and analyzed the time synchronization error impact on echo data. The time synchronization error in BiSAR comes from two separated frequency sources mounted on two separated platforms, which may cause the pulse repetition cycle of the transmitted signal not equaling the cycle of the reception window of the receiver. The main impact of the time synchronization error in BiSAR is on the arrangement of the echo data in matrix, almost no impact on azimuthal signal phase. We make use of the phase of direct-path signal to correct the time synchronization error, and on the basis of the equivalent model, we focus on azimuthal

data using time-varying step-transform algorithm. Theoretical analysis and the experimental data processing have verified that these algorithms can correct the BiSAR time synchronization error for better imaging.

REFERENCES

Chen X L, Ding C B, Liang X D and Wu Y R. 2008. An improved NLCS imaging algorithm of bistatic SAR with a stationary receiver. *Journal of Electronics & Information Technology*, **30**(5): 1041—1046

D'Aria D, Guarnieri A M and Rocca F. 2004. Focusing bistatic synthetic aperture radar using dip move out. *IEEE Trans Geosc and Remote Sens*. **42** (7): 1362—1376

Ding Y and Munson D C. 2002. Fast back projection algorithm for bistatic SAR imaging. Proc. IEEE Int. Image Process. Conf., Rochester, New York

Espeter T, Walterscheid I, Klare J and Ender JHG. 2007. Synchronization techniques for the bistatic spaceborne/airborne SAR experiment with TerraSAR-X and PAMIR. IGARSS 2007

Guo S H and Chen J. 2002. A novel method of time synchronization for bistatic radar system. *Radar & Ecm*, (4): 10—14

He F, Liang D N and Dong Z. 2005. A wavenumber domain algorithm for spaceborne bistatic SAR imaging with large squint angle. *Acta Electronica Sinica*, **33** (6): 1011—1014

Johnsen T. 2002. Time and frequency synchronization in multistatic. Radar Conference. Proceedings of the IEEE

Krieger G and Younis M. 2006. Impact of oscillator noise in bistatic and multistatic SAR. *IEEE Geoscience and Remote Sensing Letters*, **3**(3): 424—428

Rigling B D and Moses R L. 2004. Polar format algorithm for bistatic SAR. *IEEE Trans. Aerosp. Electron. Syst.*, **40** (4): 1147—1158

Sun X B, Yeo T S and Zhang C B. 1999. Time-varying step-transform algorithm for high squint SAR imaging. *Geoscience and Remote Sensing*, *IEEE Transactions on*, **37**: 2668—2677

Weiβ M. 2004. Synchronization of bistatic radar systems. IEEE International Geoscience and Remote Sensing Symposim

Zhang S K and Yang R L. 2008. A squint mode bistatic synthetic aperture radar image formation algorithm based on second range compression. *Journal of Electronics & Information Technology*, **30**(7): 1717—1721

Zhou P and Pi Y M. 2008. Study on geometry and signal model of spaceborne/airborne bi-static SAR. *Journal of Remote Sensing*, **12**(5): 750—758

Zhu Z B, Tang Z Y and Jiang X Z. 2007. The imaging algorithm of bistatic SAR with parallel track. *Journal of Electronics & Information Technology*, **29**(11): 2702—2705

机载双基地 SAR 实测数据成像

徐三元, 王建国

电子科技大学 电子工程学院, 四川 成都 610054

摘 要: 建立双基地 SAR 的单基地等效模型, 分析了系统时间同步误差的机理; 提出了双基地 SAR 回波中的直达波数据进行时间同步误差校正的算法; 在双基地 SAR 单站等效模型的基础上, 利用时变阶梯变换算法进行成像处理。经过理论分析, 实测数据处理验证, 这一算法是有效的, 能够校正双基地 SAR 时间同步误差, 较好地进行实测数据的成像处理。

关键词: 双基地, 合成孔径雷达, 时间同步, 成像算法

中图分类号: TP958 文献标识码: A

引用格式: 徐三元, 王建国. 2010. 机载双基地 SAR 实测数据成像.遥感学报, **14**(2): 262—271
Xu S Y, Wang J G. 2010. Experimental data imaging for the airborne bistatic SAR. *Journal of Remote Sensing*. **14**(2): 262—271

1 引 言

双基地 SAR(bistatic synthetic aperture radar, BiSAR)是发射机和接收机分别安装在不同运动平台上的成像雷达系统。这种平台分离特性使得其具有丰富的空时频信息, 以及灵活、隐蔽等单基地雷达不具备的优点, 具有广阔的应用前景。但由于 BiSAR 系统比单基地 SAR(monostatic synthetic aperture radar)系统复杂, 成像处理的难度也更高, 因此成了 SAR 领域近年来的研究热点(张升康 & 杨汝良, 2008; 朱振波等, 2007; 周鹏 & 皮亦鸣, 2008)。

在 BiSAR 系统中, 发射机和接收机分置在不同的平台上, 各自使用独立的频率源, 存在空间照射同步、时间同步、相位同步等方面的问题。Krieger 和 Younis (2006)研究了未补偿的相位噪声造成的影响, 旁瓣升高, 低频相位调制造成聚焦变差, 应保证相位失配在可容许的范围内。发射机的脉冲重复周期与接收机接收窗口重复周期可能不相等, 存在时间同步问题。时间同步误差的存在, 使脉冲间回波数据排列位置不能反映雷达、目标距离变化, 使雷达回波数据排列出现误差。Johnsen(2002)、Weiβ(2004)提出了利用全球定位系统、双向卫星时间传递等方法进行时间同步, 郭山红和陈菊(2002)提出一种从卫星电视信号中提取场同步信号, 以此实现时间同步的方法。德国 FGAN-FHR 开展的星机联合 SAR 技术的研究(Espeter 等, 2007), 空间—时间同步采用惯导系统(Inertial navigation system / INS)、DGPS 及 TIRA 的组合方案, 触发同步采用直达波同步技术。这些方法注重在雷达工作过程中如何保证系统时间同步。实际上, 还可以在信号处理阶段采用适当的补偿方法, 进行系统时间同步误差校正, 达到正确成像的目的。

BiSAR 的工作模式可分为非移变模式和移变模式 2 种。后向投影(BP)算法可以看成是二维匹配滤波算法的简化, 算法适应性强(Ding & Munson, 2002); 极坐标格式算法(PFA) 适应性强(Rigling & Moses, 2004) , 但成像场景较小; 非线性 chirp scaling(陈晓龙等, 2008)也应用于不同的成像模式。D'Aria 等(2004)利用地震学的波方程将双基地回波数据变换为等效的单基地 SAR 回波, 但该算法仅在 Along Track 几何布局(收发平台沿同一轨迹、同向、同速飞行)时才成立。何峰等(2005)提出了一种 BiSAR 波数域成像算法。随着斜视角的增大, 距离

收稿日期: 2009-02-05; 修订日期: 2009-05-04

基金项目: 自然科学基金 (编号: 60772144)。

第一作者简介: 徐三元 (1969—), 男, 讲师, 硕士。1993 年毕业于空军工程大学电讯工程学院, 现为电子科技大学电子工程学院在读博士研究生。主要从事合成孔径雷达系统的研究。已发表论文 5 篇。E-mail: xsy820@sohu.com。

走动急剧增大，距离走动校正使得数据矩阵有大量的零值。因此波数域算法不适处理大斜视 BiSAR。

2 BiSAR 回波模型

2.1 距离历程等效模型转换

图 1(a)即为 BiSAR 等速度平行飞行的几何模型，两个平台 S_T (发射)、S_R (接收)飞行速度相同均为 v_B，飞行高度分别为 h_T 和 h_R；设 t 为方位向时间，在 t=0 时刻，平台 S_T、S_R 和场景中心 O 之间的距离分别为 R_T、R_R，斜视角为雷达视线与雷达飞行方向之间的夹角的余角，分别为θ_T、θ_R。

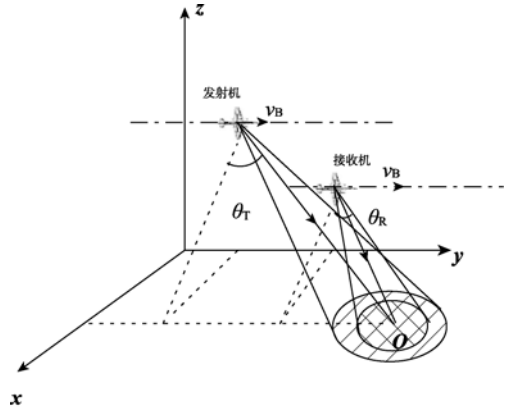

(a)

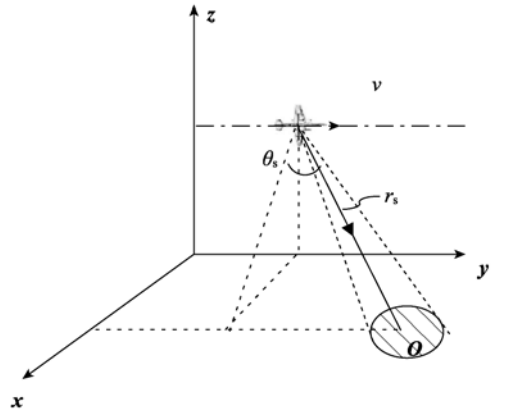

(b)

图 1 (a) 双基地 SAR 几何模型; (b) 双基地 SAR 等效模型

BiSAR 回波信号距离历程为:

$$R_B(t)=\sqrt{v_B^2t^2+R_T^2-2v_BtR_T\cos(\pi/2-\theta_T)}+\sqrt{v_B^2t^2+R_R^2-2v_BtR_R\cos(\pi/2-\theta_R)} \quad (1)$$

对(1)式进行泰勒展开

$$R_B(t)=(R_T+R_R)-(\sin\theta_T+\sin\theta_R)v_Bt+\frac{1}{2}\left(\frac{\cos^2\theta_T}{R_T}+\frac{\cos^2\theta_R}{R_R}\right)v_B^2t^2+\frac{1}{2}\left(\frac{\cos^2\theta_T\sin\theta_T}{R_T^2}+\frac{\cos^2\theta_R\sin\theta_R}{R_R^2}\right)v_B^3t^3 \quad (2)$$

非移变模式 BiSAR 系统可以近似等效为一个单基地 SAR 系统如图 1(b)。等效的单基地 SAR 在点目标 O 的回波信号单向距离历程为

$$R(t)=\sqrt{v^2t^2+r_s^2-2vtr_s\cos(\pi/2-\theta_s)}\approx r_s-vt\sin\theta_s+\frac{1}{2r_s}v^2t^2\cos^2\theta_s+\frac{1}{2r_s^2}v^3t^3\cos^2\theta_s\sin\theta_s \quad (3)$$

其中

$$\begin{cases}r_s=(R_T+R_R)/2\\ v=\dfrac{v_B}{2}\sqrt{2+2\sin\theta_T\sin\theta_R+\dfrac{R_R}{R_T}\cos^2\theta_T+\dfrac{R_T}{R_R}\cos^2\theta_R}\\ \theta_s=\sin^{-1}\left(\dfrac{v_B\sin\theta_R+v_B\sin\theta_T}{2v}\right)\end{cases} \quad (4)$$

2.2 回波信号分析

设发射机发射信号为

$$s(t,\tau)=\sum_{n=0}^{N}\mathrm{rect}\left(\frac{t-nT_s}{T}\right)\exp(\mathrm{j}2\pi(f_0\tau+K\tau^2/2)) \quad (5)$$

式中，t 为“慢时间”，是脉冲间时间，τ为“快时间”，是脉冲内时间，T 为脉冲宽度，T_s 为脉冲重复周期，f_0 为载频，K 为调频斜率。双基地 SAR 点目标到收发机的等效距离为 $R(t)$，ξ=2$R(t)$/C，C 为光速，A 为辐射强度。ξ是慢时间 t 的函数，则接收机接收的点目标回波信号为

$$s(t,\tau-\xi)=\sum_{n=0}^{N}\mathrm{A}\ \mathrm{rect}\left(\frac{t-nT_s-\xi}{T}\right)\times\exp(\mathrm{j}2\pi(f_0(\tau-\xi)+K(\tau-\xi)^2/2)) \quad (6)$$

设目标场景中有 M 个点目标，回波信号为

$$s_0(t,\tau)=\sum_{n=0}^{N}\sum_{m}^{M}A_m\mathrm{rect}\left(\frac{t-nT_s-\xi_m}{T}\right)\times\exp(\mathrm{j}2\pi(f_0(\tau-\xi_m)+K(\tau-\xi_m)^2/2)) \quad (7)$$

考虑接收窗口的影响，接收信号为

$$s_0(t,\tau)=\sum_{n=0}^{N}\mathrm{rect}\left(\frac{t-nT_r+\sigma}{T_w}\right)\times\sum_{m}^{M}A_m\mathrm{rect}\left(\frac{t-nT_s-\xi_m}{T}\right)\times\exp(\mathrm{j}2\pi(f_0(\tau-\xi_m)+K(\tau-\xi_m)^2/2)) \quad (8)$$

式中，T_r 为接收机时间窗口重复周期，T_w 为时间窗口

的宽度，σ为参考时延。对于单基地 SAR，T_r=T_s；对于双基地 SAR，T_r 可能不等于 T_s。当 T_r≠T_s 时，$n(T_r-T_s)$ 即为时间同步误差。对点目标 m，回波经过距离压缩后在数据域的位置为

$$p_m(n)=\frac{T_w}{2}+n(T_r-T_s)-\sigma-\xi_m \tag{9}$$

设 BiSAR 收发信机之间的距离为ςC，是慢时间的函数。则直达波可表示为

$$s_{rt}(t,\tau)=\sum_{n=0}^{N}\mathrm{rect}\left(\frac{t-nT_r+\sigma}{T_w}\right)A\,\mathrm{rect}\left(\frac{t-nT_s-\varsigma}{T}\right)\times \exp(\mathrm{j}2\pi(f_0(\tau-\varsigma)+K(\tau-\varsigma)^2/2)) \tag{10}$$

接收机、发射机之间的直达波，经过距离压缩后在数据域的位置为

$$p_{rt}(n)=\frac{T_w}{2}+n(T_r-T_s)-\sigma-\varsigma \tag{11}$$

从表达式可见，直达波在数据域的位置同样受到时间同步误差 $n(T_r-T_s)$和距离时延的影响。

3 BiSAR 时间同步误差校正

由于直达波信号强度较高，受其他目标回波影响小，方便距离校正和方位相位提取，因此采用下面的算法进行时间同步误差校正。第一次距离校正，将距离压缩后的直达波校正到同一距离门，即将直达波信号搬移为按照直线排列，相当于消除了雷达平台之间的距离变化和同步误差，其他目标的距离向位置也相应变化。

直达波经过距离压缩后在数据域的位置为

$$\begin{aligned}p'_{rt}(n)&=\left\{\frac{T_w}{2}+n(T_r-T_s)-\sigma-\varsigma\right\}-\left\{n(T_r-T_s)-\varsigma\right\}\\&=\frac{T_w}{2}-\sigma\end{aligned} \tag{12}$$

其他目标回波经过距离压缩后在数据域的位置为

$$\begin{aligned}p'_m(n)&=\left\{\frac{T_w}{2}+n(T_r-T_s)-\sigma-\xi_m\right\}-\left\{n(T_r-T_s)-\varsigma\right\}\\&=\left\{\frac{T_w}{2}-\sigma-\xi_m\right\}+\varsigma\end{aligned} \tag{13}$$

再沿方位向取出直达波随慢时间变化的相位，获得收发信机之间的相对距离。直达波的方位向相位为 phase=$-2\pi f_0\varsigma$，可得ς=−phase/$2\pi f_0$。

第二次距离校正，将校直后的信号按照ς到的变化再次校正信号位置，得到直达波经过距离压缩后在数据域的位置为

$$p''_{rt}(n)=\frac{T_w}{2}-\sigma-\varsigma \tag{14}$$

其他目标回波经过距离压缩后在数据域的位置为

$$p''_m(n)=\frac{T_w}{2}-\sigma-\xi_m \tag{15}$$

这样，距离压缩后的数据排列位置决定与雷达平台与目标之间的距离变化，不再受同步误差的影响，时间同步误差被校正了。流程如图 2 。

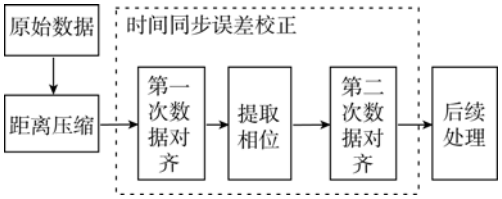

图 2　双基地 SAR 时间同步误差校正

4 BiSAR 时变阶梯变换算法

在斜视情况下，斜距变化比方位聚焦深度大得多，这意味着对同一目标，只有合成孔径时间内的小部分能够用同一参考信号聚焦，时变的子孔径成像技术适应大距离走动的斜视 SAR 成像处理(Sun 等, 1999)。完成距离压缩后，需要对数据矩阵进行距离迁移校正。经过校正的数据，可以认为同一目标的方位回波数据已经在同一个斜距单元。方位向处理第一步需要进行线性相位补偿。分子孔径作去斜处理，作去斜处理时，每个子孔径采用不同的参考函数，即时变的参考函数。对子孔径去斜信号作 FFT，得到粗分辨率的数据，将若干个子孔径数据顺序排成一个矩阵，沿对角线方向进行数据挑选，获得目标的全孔径数据，对挑选数据进行子孔径间相位补偿，再作精分辨率 FFT。由于子孔径间为防止栅瓣效应必须有重叠，因此，对精分辨率 FFT 的输出信号还要进行数据挑选。整个算法流程框图如图 3。

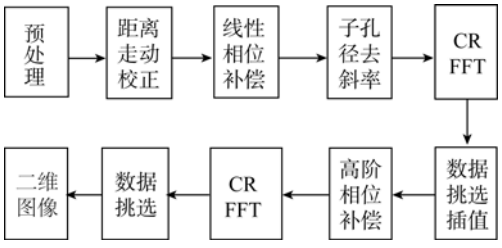

图 3　时变阶梯变换算法

5 BiSAR 实测数据处理

图 4 是某次实验实测数据经过距离压缩后时间同步误差校正前的图像。图 5 为从提取的直达波方

位向相位历程中计算得到的反映了 BiSAR 收发平台相对距离变化。图 6 为距离压缩后时间同步误差校正后的图像。经过图 3 所示时间同步误差校正后，进行时变阶梯变换处理，最后得到图 7 的灰度图。

从图 4 可以看出，由于时间同步误差的存在，回波在数据域的排列不能直接反映距离的变化，图

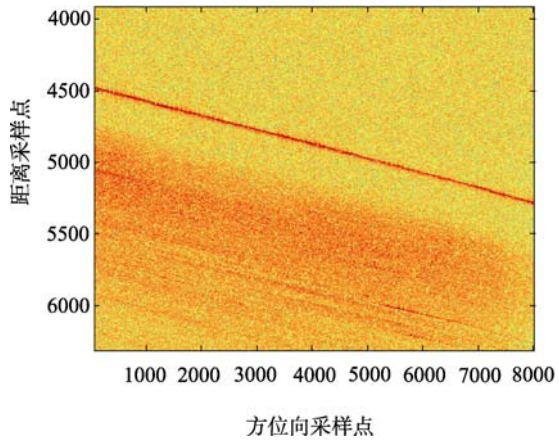

图 4 距离压缩后的 SAR 数据

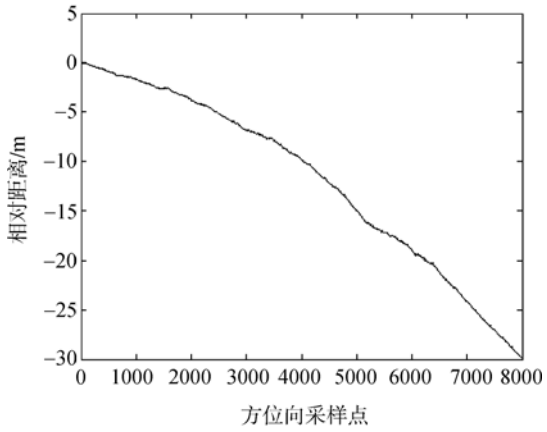

图 5 直达波反映的距离变化历程

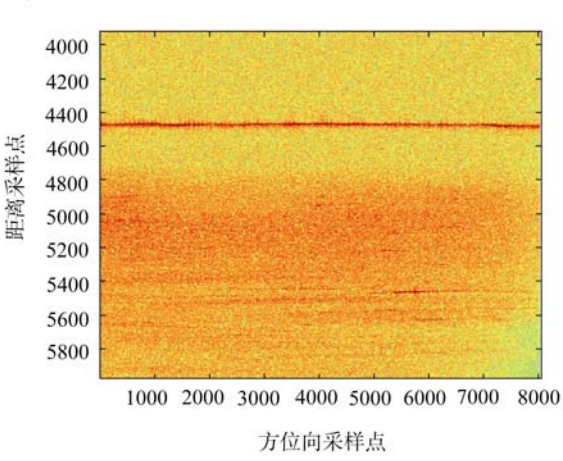

图 6 时间同步误差校正后的 SAR 数据

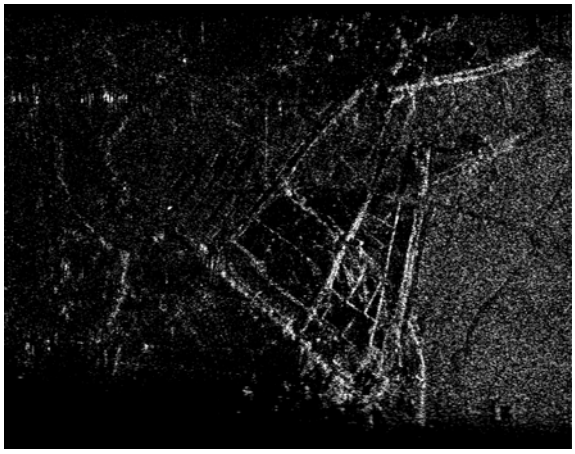

图 7 实测数据成像结果

中较强的曲线为直达波距离压缩后的图像。直达波的位置移动最多将近 850 个距离分辨单元。如图 5，BiSAR 的 2 个平台相对距离发生变化，距离在观测过程中缩小了近 30 m，约 20 个距离分辨单元。因为平台的相对运动不能忽略，所以不能仅仅根据直达波的轨迹直接将场景回波对齐拉直，必须将平台运动和时间误差造成的影响区分开。如图 7，由于同步误差的影响，部分场景数据不全，有信息丢失。

另外，由于在进行时间同步误差校正时利用了收发信机之间的直达波相位，获得 2 个平台相对距离。在这一操作过程中，若平台相对距离变化过于剧烈，如飞机转弯时，超过方位向采样频率即 PRF 允许的范围时，则取得的直达波相位不能反映平台相对距离的变化，同步误差校正算法失效，但这时通常也不适宜测绘成像。

6 结 论

在 BiSAR 系统中，目标回波信号斜距历程与单基地 SAR 存在本质差异，因而单基地成像算法无法直接应用于双基地系统。本文建立了 BiSAR 的单基地等效模型，分析了回波数据受到系统时间同步误差的影响；系统时间同步误差是由于发射机和接收机分置在不同的平台上，各自使用独立的频率源，发射机的脉冲重复周期与接收机接收窗口重复周期不相等造成的；时间同步误差主要影响回波数据的位置排列，不影响回波的方位相位；利用 BiSAR 回波中的直达波数据进行时间同步误差校正；在 BiSAR 单站等效模型的基础上，利用时变阶梯变换算法进行成像处理。经过理论分析，实测数据处理验证，这一算法是有效的，能够校正 BiSAR 时间同步误差，进行较好的成像处理。

REFERENCES

Chen X L, Ding C B, Liang X D and Wu Y R. 2008. An improved NLCS imaging algorithm of bistatic SAR with a stationary receiver. *Journal of Electronics & Information Technology*, **30**(5): 1041—1046

D'Aria D, Guarnieri A M and Rocca F. 2004. Focusing bistatic synthetic aperture radar using dip move out. *IEEE Trans Geosc and Remote Sens*. **42** (7): 1362—1376

Ding Y and Munson D C. 2002. Fast back projection algorithm for bistatic SAR imaging. Proc. IEEE Int. Image Process. Conf., Rochester, New York

Espeter T, Walterscheid I, Klare J and Ender JHG. 2007. Synchronization techniques for the bistatic spaceborne/airborne SAR experiment with TerraSAR-X and PAMIR. IGARSS 2007

Guo S H and Chen J. 2002. A novel method of time synchronization for bistatic radar system. *Radar & Ecm*, (4): 10—14

He F, Liang D N and Dong Z. 2005. A wavenumber domain algorithm for spaceborne bistatic SAR imaging with large squint angle. *Acta Electronica Sinica*, **33** (6): 1011—1014

Johnsen T. 2002. Time and frequency synchronization in multistatic. Radar Conference. Proceedings of the IEEE

Krieger G and Younis M. 2006. Impact of oscillator noise in bistatic and multistatic SAR. *IEEE Geoscience and Remote Sensing Letters*, **3**(3): 424—428

Rigling B D and Moses R L. 2004. Polar format algorithm for bistatic SAR. *IEEE Trans. Aerosp. Electron. Syst.*, **40** (4): 1147—1158

Sun X B, Yeo T S and Zhang C B. 1999. Time-varying step-transform algorithm for high squint SAR imaging. *Geoscience and Remote Sensing, IEEE Transactions on*, **37**: 2668—2677

Weiβ M. 2004. Synchronization of bistatic radar systems. IEEE International Geoscience and Remote Sensing Symposim

Zhang S K and Yang R L. 2008. A squint mode bistatic synthetic aperture radar image formation algorithm based on second range compression. *Journal of Electronics & Information Technology*, **30**(7): 1717—1721

Zhou P and Pi Y M. 2008. Study on geometry and signal model of spaceborne/airborne bi-static SAR. *Journal of Remote Sensing*, **12**(5): 750—758

Zhu Z B, Tang Z Y and Jiang X Z. 2007. The imaging algorithm of bistatic SAR with parallel track. *Journal of Electronics & Information Technology*, **29**(11): 2702—2705

附中文参考文献

陈晓龙, 丁赤飚, 梁兴东, 吴一戎. 2008. 改进的接收机固定双站 NLCS 成像方法.电子信息学报, **30**(5): 1041—1046

郭山红, 陈菊. 2002. 实现双/ 多基地雷达时间同步的一种新方法. 雷达与对抗, (4): 10—14

何峰, 梁甸农, 董臻. 2005. 适于大斜视角的量载双基地 SAR 波数域成像算法. 电子学报, **33**(6): 1011—1014

张升康, 杨汝良. 2008. 基于二次距离压缩的双基地合成孔径雷达斜视成像算法. 电子与信息学报. **30**(7): 1717—1721

周鹏, 皮亦鸣. 2008. 星机双基地 SAR 空间几何关系与信号模型. 遥感学报, **12**(5): 750—758

朱振波, 汤子跃, 蒋兴舟. 2007. 平飞模式双站 SAR 成像算法研究. 电子信息学报, **29**(11): 2702—2705